

Fig. 1: Analyzed electrical system.

Modelling

The models of the studied electrical system have been implemented in Mathworks Simulink software. The small-signal models of the converters were created on the basis of the dq-transformations concept. These models are sufficient for a design and analysis of the control system [5, 6].

VSI model

The average model of the VSI system is derived by the equations (1) – (4) below :

$$\frac{dI_{id}}{dt} = -\frac{R}{L}I_{id} + \omega I_{iq} - \frac{1}{L}V_{cd} + \frac{1}{2L}V_{dc_i}m_d \quad (1)$$

$$\frac{dI_{iq}}{dt} = -\frac{R}{L}I_{iq} - \omega I_{id} - \frac{1}{L}V_{cq} + \frac{1}{2L}V_{dc_i}m_q \quad (2)$$

$$\frac{dV_{cd}}{dt} = \frac{1}{C}I_{id} + \omega V_{cq} - \frac{1}{C}I_{ad} \quad (3)$$

$$\frac{dV_{cq}}{dt} = \frac{1}{C}I_{iq} - \omega V_{cd} - \frac{1}{C}I_{aq} \quad (4)$$

L, C, R are the VSI output filter inductance, capacitance and parasitic resistance respectively. I_{id}, I_{iq} are the output inductance current in its dq-frames, V_{cd}, V_{cq} are the output capacitor voltage in its dq-frames. m_d and m_q are modulation indexes in dq-frame respectively, ω is the AC supply angular frequency, V_{dc_i} is the VSI dc voltage and it is assumed to be constant.

AFE model

The average model of the AFE system with a resistive load on its DC side is derived by the equations (5) – (7) below :

$$\frac{dI_{ad}}{dt} = -\frac{R_a}{L_a}I_{ad} + \frac{1}{L_a}V_{cd} + \omega I_{aq} - \frac{1}{2L_a}V_{dc_a}p_d \quad (5)$$

$$\frac{dI_{aq}}{dt} = -\frac{R_a}{L_a}I_{aq} + \frac{1}{L_a}V_{cq} - \omega I_{ad} - \frac{1}{2L_a}V_{dc_a}p_q \quad (6)$$

$$\frac{dV_{dc_a}}{dt} = \frac{3}{4C_a}I_{ad}p_d + \frac{3}{4C_a}I_{aq}p_q - \frac{1}{C_a R_L}V_{dc_a} \quad (7)$$

L_a, R_a are the AFE input filter inductance and parasitic resistance, C_a is the AFE output capacitance, I_{ad}, I_{aq} are the input inductance current in its dq-frames, V_{dc_a} is the dc-link output voltage, p_d and p_q are modulation indexes in dq-frame respectively, ω is the AC grid angular frequency, R_L is a dc side resistive load.

The converters' filters values have been designed on the basis of power quality standards requirements in the nominal operating point. The system rated parameters are presented in the table below (Table I).

Table I: System nominal parameters

VSI	AFE
$P_N = 1.5 \text{ kW}$	$P_N = 1.5 \text{ kW}$
$V_{in} = 350 \text{ V dc}$	$V_{in} = 115 \text{ V AC rms}$
$V_{out} = 115 \text{ [V] AC rms}$	$V_{out} = 350 \text{ V dc}$
$f_n = 400 \text{ Hz}$	–
$L = 230.4 \text{ } \mu\text{H}$	$L_a = 636.3 \text{ } \mu\text{H}$
$C = 31.8 \text{ } \mu\text{F}$	$C_a = 100 \text{ } \mu\text{F}$
$f_{sw} = 20 \text{ kHz}$	$f_{sw} = 20 \text{ kHz}$
Controller bandwidths	
$f_i = 1000 \text{ Hz}$	$f_i = 600 \text{ Hz}$
$f_v = 100 \text{ Hz}$	$f_v = 40 \text{ Hz}$

Controller Design

The designed converters control system consists of 4 control loops containing PI controllers. Two for controlling VSI output voltage and current (V_{cd} and I_{iq}), other two control AFE output voltage and current (V_{dc_a} and I_{aq}). V_{cd} and V_{dc_a} are set to the nominal values references $V_{cd} = 162.6 \text{ V}$ (115 V rms), $V_{dc} = 350 \text{ V dc}$ accordingly. I_{iq} and I_{aq} are set to 0 in order to keep unity power factor. The control design has been carried out individually for each converter, the appropriate gains calculation for each PI controller is derived below.

VSI controller

VSI PI controller gains are calculated by using the following equations (8) – (11)

$$K_{pv_{VSI}} = 2\zeta C f_{v_{VSI}} 2\pi \quad (8)$$

$$K_{iv_{VSI}} = C (f_{v_{VSI}} 2\pi)^2 \quad (9)$$

$$K_{pi_{VSI}} = 2\zeta L f_{i_{VSI}} 2\pi - R \quad (10)$$

$$K_{ii_{VSI}} = L (f_{i_{VSI}} 2\pi)^2 \quad (11)$$

$K_{pv_{VSI}}$ and $K_{iv_{VSI}}$ are proportional and integral gains for VSI voltage loop PI controller, $K_{pi_{VSI}}$ and $K_{ii_{VSI}}$ are proportional and integral gains for VSI current loop. $f_{v_{VSI}}$ and $f_{i_{VSI}}$ are voltage and current loop controller bandwidths accordingly. ζ is a damping factor and is set to one in the whole analysis.

AFE controller

AFE PI controller gains are calculated by using the following equations (12) – (15)

$$K_{pv_{AFE}} = 2\zeta C_a f_{v_{AFE}} 2\pi \quad (12)$$

$$K_{iv_{AFE}} = C_a (f_{v_{AFE}} 2\pi)^2 \quad (13)$$

$$K_{pi_{AFE}} = -2\zeta L_a f_{i_{AFE}} 2\pi - R_a \quad (14)$$

$$K_{ii_{AFE}} = -L_a (f_{i_{AFE}} 2\pi)^2 \quad (15)$$

$K_{pv_{AFE}}$ and $K_{iv_{AFE}}$ are proportional and integral gains for AFE voltage loop PI controller, $K_{pi_{VSI}}$ and $K_{ii_{VSI}}$ are proportional and integral gains for VSI current loop. $f_{v_{AFE}}$ and $f_{i_{AFE}}$ are voltage and current loop controller bandwidths accordingly.

The simulation using dq frame representation allowed to verify whether the system meets the control requirements. The designed system based on the nominal parameters of the filters meets DO160 and MIL704F standards. The simulation results presenting output currents and voltages waveforms of the designed electrical system with PI control strategy are depicted in the Fig. 2. Figure shows dynamic behaviour of the system where the resistive load $R_L=80 \Omega$ is connected at 0.2 s.

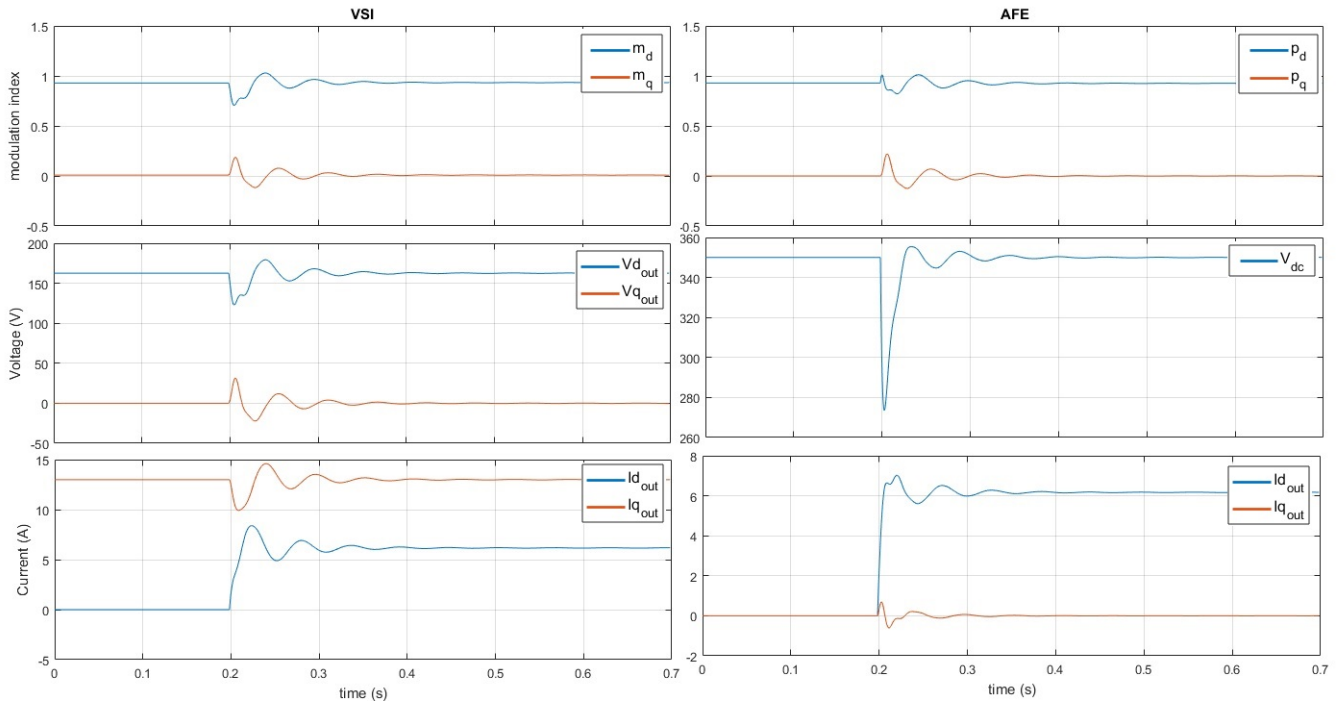


Fig. 2: VSI and AFE waveforms in dq frame.

Dynamic Behaviour Analysis

The study of the passive components influence on the global behaviour of the system was performed with using the average model. In order to analyse this influence different sets of the VSI LC filter and AFE L and C filters parameters have been tested. Afterwards, the system dynamic behaviour such as both converters output voltages, voltage overshoots, undershoots and settling times for each set have been compared with the standards. The analysis has revealed that the components which have a significant influence on the global control system are the capacitors of the VSI LC filter and inductors of the AFE L filter. By reducing their values the control system performance is decreased.

Fig. 3 presents the simulation results of the dynamic behaviour analysis. The resistive load $R_L=80 \Omega$ was connected in each test at time 0.5s. Fig. 3a, Fig. 3b and Fig. 3c present VSI and AFE output voltages waveforms for different LC filter cutoff frequencies, specifically, different LC capacitors values, since they have major influence on the dynamic behaviour. Each figure presents output voltages waveforms for different value of the AFE L filter. Moreover, the dynamic performance limitations defined by the standard MIL704F are marked as red lines.

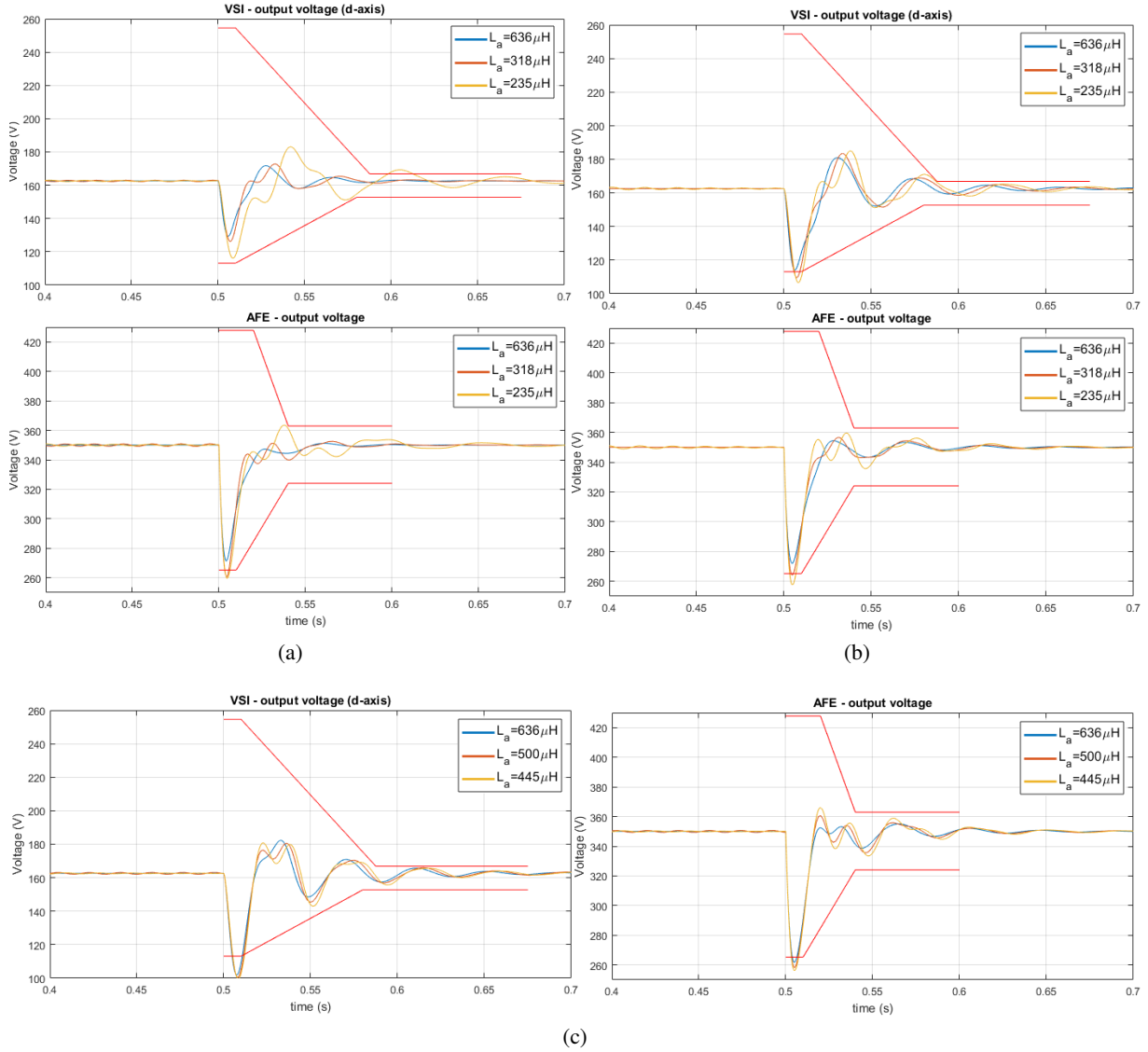


Fig. 3: VSI and AFE output voltages for a different LC filter cutoff frequency
a) $f_c=1861\text{Hz}$ b) $f_c=2151\text{Hz}$ c) $f_c=2358\text{Hz}$.

The simulation results showed that increasing the LC filter cutoff frequency decrease the global system performance so the flexibility of changing the AFE boost inductor L_a in order to maintain requirements met. In the case when cutoff frequency $f_c=2358\text{ Hz}$, the system dynamic behaviour does not meet the requirements even with the nominal value of the AFE boost inductor $L_a=636.3\text{ }\mu\text{H}$. It implies that individually designed converters' controllers which meets the requirements, might not meet the requirements when converters are connected together. This specifically underlines the need of considering both converters when designing the controller of each individual converter [7]. One of the solutions might be to increase the controllers bandwidths [8][9], however, they are limited by the sampling frequency of the controlling unit e.g. FPGA/DSP.

Experimental Measurements

In order to verify the simulation results, a prototype VSI-AFE rig has been built (Fig. 4). During the test similar filter parameters to the those used in the simulation has been used, however, due to limitations of the VSI converter (max. input voltage 300 V dc) its reference output voltage has been set to 80 V rms instead of 115 V rms. Otherwise, the VSI controller would be saturated when supplying the VSI with 300V dc. Moreover, the resistive load has been changed to $R_L=19.4 \Omega$. The passive filter parameters which have been used in the tests are $L=245 \mu\text{H}$, $C=33 \mu\text{F}$, $C=16 \mu\text{F}$, $L_a=595 \mu\text{H}$, $L_a=345 \mu\text{H}$ and $C_a=100 \mu\text{H}$. The controller bandwidths had to be reduced due to FPGA/DSP limitations to $f_{i_{VSI}}=800 \text{ Hz}$, $f_{v_{VSI}}=80 \text{ Hz}$, $f_{i_{AFE}}=500 \text{ Hz}$ and $f_{v_{AFE}}=30 \text{ Hz}$. The measurements have been performed with using ADC channels of the controller.

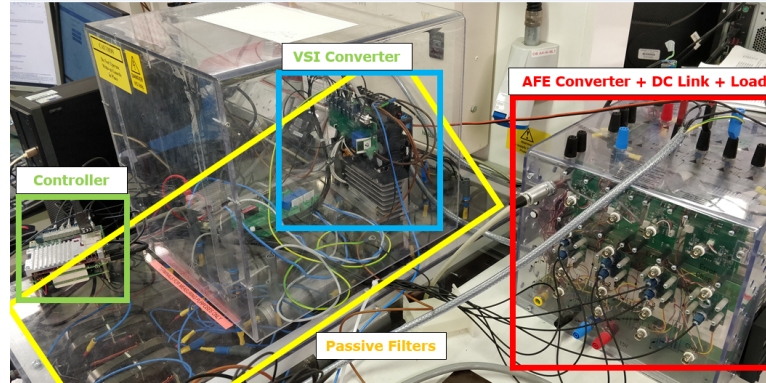


Fig. 4: The prototype rig view.

The Fig. 5 presents experimental results of the dynamic behaviour analysis. The waveforms present the transient of the load connection. Fig. 5a and Fig. 5b present VSI and AFE output voltages waveforms for different LC filter cutoff frequencies $f_c=1770 \text{ Hz}$ ($C=33 \mu\text{F}$) and $f_c=2542 \text{ Hz}$ ($C=16 \mu\text{F}$). Moreover, in each figure waveforms for different value of AFE L filter ($L_a=595 \mu\text{H}$ and $L_a=345 \mu\text{H}$). The system requirements could not be checked in the experiments since they are defined for 115 V rms.

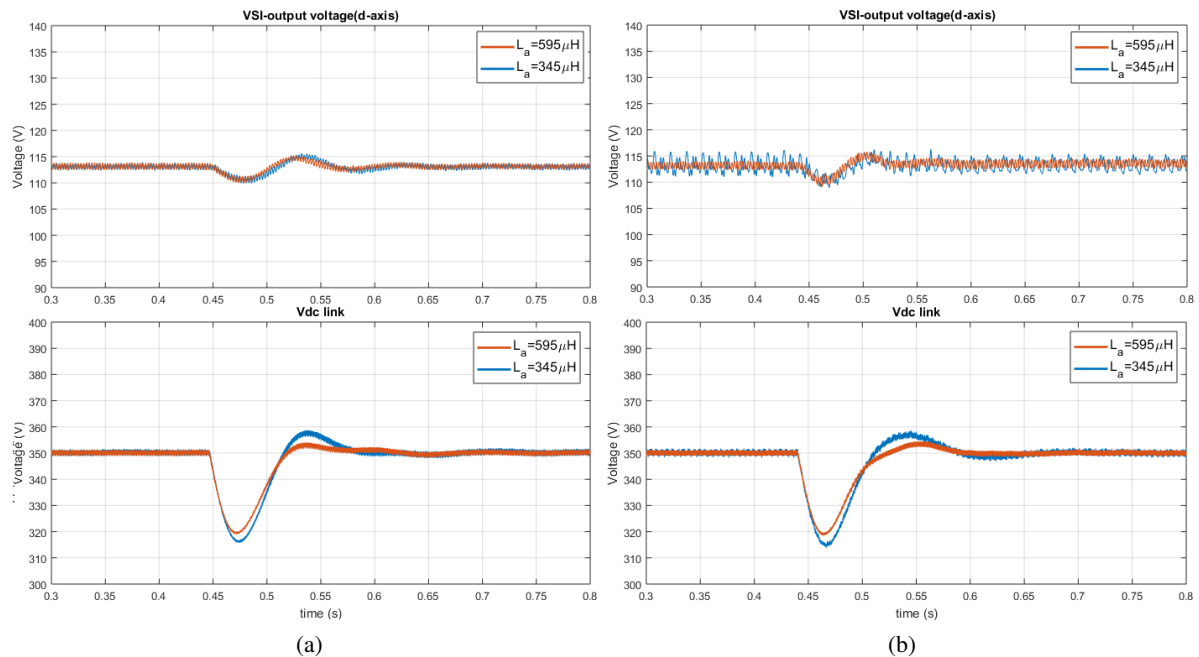


Fig. 5: Experiment results. VSI and AFE output voltages for a different LC filter cutoff frequency
a) $f_c=1770 \text{ Hz}$ b) $f_c=2542 \text{ Hz}$.

The experiments results show the same trend to the ones obtained from the simulation, however, the changes for different sets of passive filters are lesser due to decreased values of the VSI output voltage and resistive load. Moreover, for smaller values of the filters components output voltages are more distorted so the differences are even harder to recognize. Nevertheless, we can see that increasing VSI LC filter cutoff frequency and decreasing AFE boost inductor affects the global system performance.

Conclusion

The analysis carried out in this work has revealed that the coupling between two converters affects the control performance. Due to that, both converters with individually designed control systems might not meet requirements when they are connected together. Therefore, it is necessary to either consider whole system in the control design process or design the global system controller in order to meet the aircraft requirements. To sum up, using a standard controller approach like PI, PID could not sufficient in some cases due to bandwidth or dynamic behaviour limitations. Thus, it is advised to use advanced control strategies such as LQR and H2 which represents much better performance [10].

References

- [1] X. Roboam, B. Sareni, and A. De Andrade, More electricity in the air: Toward optimized electrical networks embedded in more-electrical aircraft, *IEEE industrial electronics magazine*, vol. 6, no. 4, pp. 617, 2012.
- [2] P. Wheeler, S. Bozhko, "The more electric aircraft: technology and challenges", *Electrification Magazine IEEE*, vol. 2, no. 4, 2014.
- [3] X. Roboam, New Trends and Challenges of Electrical Networks embedded in "More Electric Aircraft", in *IEEE International Symposium on Industrial Electronics*, Gdansk, 2011.
- [4] Y. Wang, M. Yin, and F. Gao, Control design of paralleled source in electrical power systems of more-electric aircraft, in *Proc. IEEE Int. Conf. Aircraft Utility Syst. (AUS)*, Beijing, China, Oct. 2016, pp. 664669.
- [5] B. Wen, D. Boroyevich, R. Burgos, P. Mattavelli, and Z. Shen, Analysis of dq small-signal impedance of grid-tied inverters, *IEEE Transactions on Power Electronics*, vol. 31, no. 1, pp. 675687, 2016.
- [6] S. Hiti, D. Boroyevich and C. Cuadros, Small-Signal Modeling and Control of Three-Phase PWM Converters, in *Industry Applications Society Annual Meeting, 1994.*, Conference Record of the 1994 IEEE, Denver, Colorado, 1994.
- [7] K. Areerak, *Modelling and Stability Analysis of Aircraft Power Systems*, The University of Nottingham, 2009
- [8] B. Wen, *Stability Analysis of Three-Phase AC Power Systems Based on Measured D-Q Frame Impedences*, Virginia Polytechnic and State University, Blacksburg, Virginia, 2014.
- [9] Q. Li, A. Formentini, A. Baraston, X. Zhang, P. Zanchetta, J.-L. Schanen, and D. Boroyevich, Taking into account interactions between converters in the design of aircraft power networks, in *Energy Conversion Congress and Exposition (ECCE), 2016 IEEE*. IEEE, 2016, pp. 17.
- [10] A. Formentini, D. Dewar, P. Zanchetta, P. Wheeler, D. Boroyevich, and J.-L. Schanen, Optimal control of three-phase embedded power grids, in *Control and Modeling for Power Electronics (COMPEL), 2016 IEEE 17th Workshop on*. IEEE, 2016, pp. 16.